



1 **A lesson in preparedness: Assessing the effectiveness of low-cost post-**
2 **wildfire flood protection measures for the catastrophic flood in**
3 **Kineta, Greece**

4 George Papaioannou¹, Angelos Alamanos², Mohammed Basheer³, Nikolaos Nagkoulis⁴, Vassiliki
5 Markogianni⁵, George Varlas⁵, Angelos Plataniotis^{6,7}, Anastasios Papadopoulos⁵, Elias Dimitriou⁵ and
6 Phoebe Koundouri^{4,7,8}

7 ¹ Department of Forestry and Management of the Environment and Natural Resources, Democritus University of Thrace,
8 68200 Orestiada, Greece

9 ² Independent Researcher, Berlin, 10243, Germany

10 ³ Department of Civil & Mineral Engineering, University of Toronto, Toronto, Ontario, Canada

11 ⁴ School of Economics and ReSEES Research Laboratory, Athens University of Economics and Business, Athens 10434,
12 Greece

13 ⁵ Hellenic Centre for Marine Research, Institute of Marine Biological Resources and Inland Waters, Anavissos, 19013 Attiki,
14 Greece

15 ⁶ National and Kapodistrian University of Athens, Athens, Greece

16 ⁷ UN SDSN (Global Climate Hub, European Hub, Greek Hub), Athens, Greece

17 ⁸ Department of Technology, Management and Economics, Denmark Technical University (DTU), Kongens Lyngby 2800,
18 Denmark

19 *Correspondence to:* George Papaioannou (gpapaio@fmenr.duth.gr)

20 **Abstract.** Climate change–driven wildfires, especially in the Mediterranean, are not only becoming more frequent and severe
21 but also amplifying flood risks by altering catchment hydrology. Yet, post-fire flood risk management remains inadequately
22 addressed. In response, we develop an integrated simulation framework that combines meteorological, hydrological, hydraulic-
23 hydrodynamic models and remote sensing techniques to represent post-wildfire flood hazards and support the design of Post-
24 wildfire Flood Protection Treatments (PFPTs). We utilize the framework to accurately represent a post-wildfire flash flood
25 event in a Mediterranean catchment in Greece. The flood event is simulated under three scenarios: pre-wildfire, post-wildfire
26 without any PFPTs in place (reality), and post-wildfire with PFPTs. The results show that the wildfire's impact on flood extent
27 was around a 24.1% increase, but the PFPTs could have counterbalanced this impact. Moreover, we present an economic
28 model for estimating the cost of the recommended PFPTs and the flood damage direct costs, combining an accounting and a
29 semi-automated AI-based approach. The cost comparison reveals that the protection would have cost around €3.45mill (just
30 the 13.7% of the flood damage costs, €25.2mill) potentially saving €6.37mill in flood damage. By filling critical knowledge
31 gaps, our study offers insights into the dynamics of post-wildfire flood events and provides policymakers with valuable insights
32 for timely risk mitigation amidst escalating fire-related disasters.



33 **Keywords:** Wildfires; Flood protection; Barrier treatments; In-channel treatments; Hydraulic modelling; Rain-on-Grid;
34 Meteorological modelling; Remote Sensing; Protection Cost.

35

36 **1 Introduction**

37 The escalating frequency and intensity of wildfires, attributed to climate change, present an unprecedented challenge with
38 widespread and complex ramifications for both ecosystems and human populations (Wang et al., 2020). Although wildfires
39 are most prevalent during summer periods, the associated damages persist longer, posing severe risks (Brogan et al., 2019b,
40 a). Wildfires can cause substantial alterations in vegetation, soil conditions, land cover, hydromorphology, and the hydrological
41 response of burnt catchments during storm events (Alamanos, 2024; Hasan et al., 2020). The implications become apparent
42 when the first extreme storms occur, and the burned sites are found to be more vulnerable to flash floods due to their reduced
43 infiltration capacity, sensitivity to peak flows, and increased runoff and sediment transport loads (Havel et al., 2018). The
44 Mediterranean region, a climate change hotspot, has been particularly vulnerable to increasingly severe wildfires and flood
45 events over the last few years, and such threats are anticipated to become more prevalent in the future (Cos et al., 2022). Thus,
46 it is imperative to better understand the dynamics of such risks and to be proactive through continuous resilience-building
47 efforts. A better understanding of fire-flood dynamics and their effects can be achieved through data-driven models, which
48 explore the flooding response in burned sites. Resilience-building efforts after a wildfire involve, at a minimum, treatments to
49 protect the burned sites from extreme runoff and soil erosion. The cost and effectiveness of these approaches for enhancing
50 preparedness for flood hazards are scrutinized in this paper.

51 Data-driven approaches for evaluating the flood impacts of wildfires include hydrological simulations of post-wildfire runoff
52 and flood mapping of burnt sites. The former is more common and focuses on how wildfires change soil and hydrological
53 properties, how they recover, or even perform experiments to quantify the differences in hydrological responses (Ebel and
54 Martin, 2017). The latter includes only a few applications in the literature, as such models are data-intensive. Typically, these
55 models simulate various storms, aiming to present different risk scenarios. Theochari and Baltas (2022) analyzed the
56 hydrological and hydraulic responses of flood-prone areas in a burned site on Evia Island, Greece, to a design storm. Godara
57 et al. (2023) applied the hydraulic model Telemac to investigate how a Norwegian catchment responds to a design flood.
58 Chrysovergis et al. (2021) studied a real post-wildfire event that caused flood and erosion damages in Southern California,
59 with the focus being on the factors that caused the damages. These studies indicate that burnt areas are more vulnerable to
60 flash floods due to increased soil imperviousness and peak discharge, underscoring the necessity for accurate models for flood
61 inundation mapping and assessing post-wildfire protection measures. However, such studies are very scarce in the literature.
62 Post-wildfire Flood Protection Treatments (PFPTs) aim to protect burned areas from flooding and other hazards, such as
63 landslides and soil erosion, which are linked to extreme precipitation (Basheer and Oommen, 2024). PFPTs include several
64 interventions that are case-specific, depending on the site's physical characteristics. PFPTs include barriers, mulch or



65 hydromulch, and seeding (aiming for a quicker recovery of the burnt area), slit fences, erosion control mats, or the installation
66 of in-channel structures (e.g., trees, log-erosion barriers, check dams) to 'cut' excess runoff and debris flows. The main and
67 most common PFPT types, according to Napper (2006) and Papaioannou et al. (2023), are the land treatments (installing
68 barriers to reduce runoff and erosion), and channel treatments (in-stream interventions for water control). Barrier-based land
69 treatments are more suitable for areas with high to moderate burn severity and slopes of up to 60%. Channel treatments, on the
70 other hand, are more suitable for areas with high burn severity and smooth slopes, ensuring site accessibility for maintenance
71 and inspection. There is a lack of studies on the performance of PFPTs, with the majority of the studied cases being in the US,
72 Spain and Portugal (Girona-García et al., 2021). While there are some studies on the application of PFPTs, these primarily
73 refer to specific types of measures, mostly focusing on soil erosion rather than flood hazards, and are highly case-specific
74 (Girona-García et al., 2023; Robinne et al., 2020). In one of the few examples evaluating the effectiveness of PFPTs, Kastridis
75 and Kamperidou (2015) focus on two northern Greek basins, where the applied measures included cutting burned trees, a total
76 ban on grazing, and the construction of log erosion barriers, log check-dams, and contour branch barriers. They observed
77 failures of these PFPTs, mainly due to the rush of construction and their poor implementation, which resulted in subsequent
78 floods. The importance of the timely and proper installation of PFPTs to enhance their efficiency in mitigating flood risks is
79 also highlighted by Mitsopoulos et al. (2022), studying another Greek burnt site. A similar study (Posner and Georgakakos,
80 2017) evaluated the feasibility and impact of check-dams (gabion-dams) and vegetation coverage PFPTs in the mountainous
81 areas of Haiti, indicating that hillslope revegetation primarily impacts lower return period storms, while channel vegetation
82 reduces peak discharge and delays flood peaks, and combined gabion dams and channel vegetation effects are non-linear and
83 dependent on storm characteristics. But, to the best of our knowledge, no study simulates a real post-wildfire flood event along
84 with suitable PFPTs to test the effects of the fire and the role of PFPTs in the actual flooding. Even more scarce in the academic
85 literature are studies evaluating the PFPT costs, considering various components from installation to material and labour costs,
86 probably due to the case- and context-specific nature of this problem. These costs are often cited as the greatest obstacle to
87 their implementation.

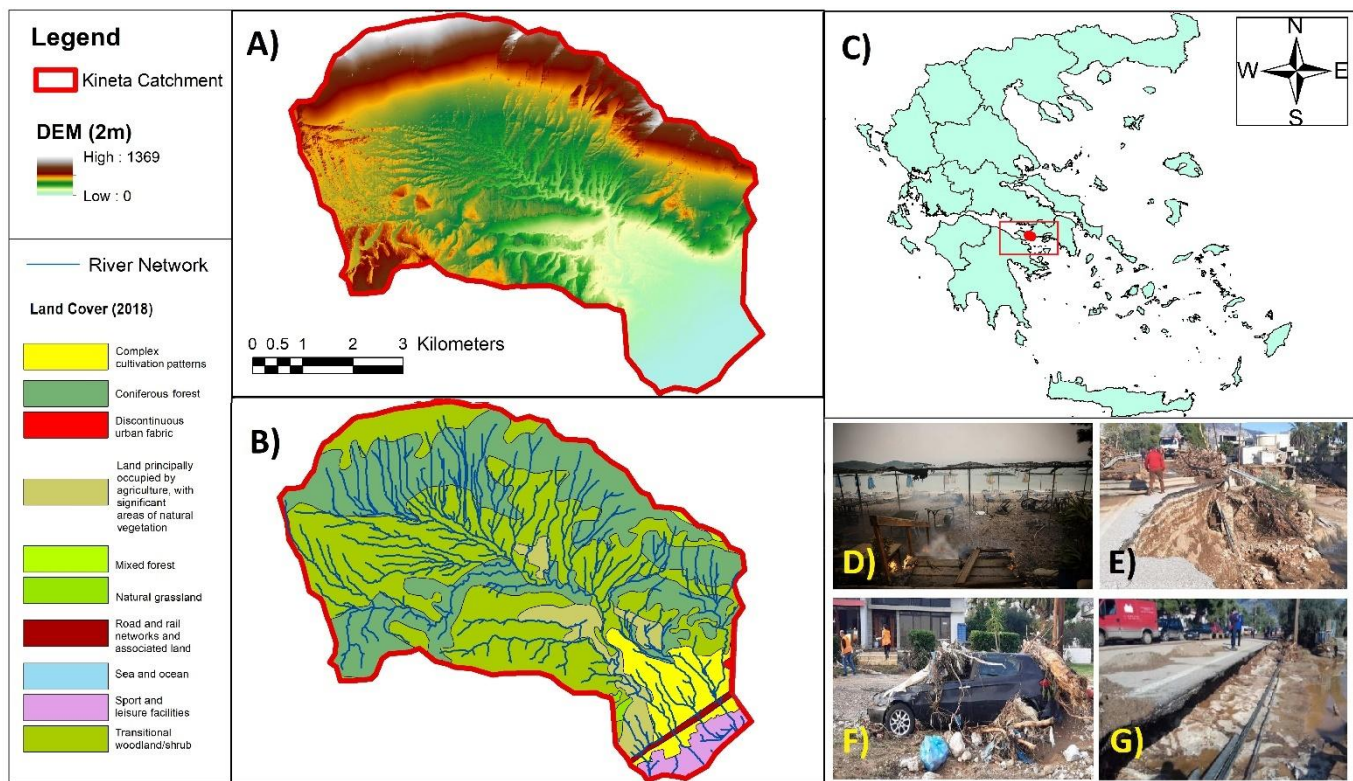
88 Reflecting on the above, there are three apparent research gaps. First, there are very few studies on the response of burned sites
89 to real flood events, as simulated by hydraulic models. Second, the role of PFPTs remains under-explored, and despite some
90 general (national) guidelines for the selection and installation of certain treatments, there is still room for improvement in
91 simulating and assessing their effectiveness and associated economic implications (Papaioannou et al., 2023). Third, the costs
92 associated with applying the necessary PFPTs, and especially their comparison with the flood damage costs that can occur, are
93 a crucial analysis to reveal whether and how beneficial the PFPTs can be for building flood resilience. In this paper, we aim
94 to cover these three gaps by: i) a detailed representation of a post-wildfire flood event in a typical Mediterranean site, based
95 on our previous works combining atmospheric model with remote sensing and hydraulic modelling (Alamanos et al., 2024b;
96 Varlas et al., 2024). ii) Assessing the most appropriate PFPTs and modelling them spatially. iii) Assessing their effectiveness
97 for flood mitigation, by directly incorporating them in the hydraulic model. iv) Estimating their costs, as well as comparing them
98 with the estimated direct flood damage costs. Each one of these analyses, and especially their combination, is a novel



99 contribution with direct practical and policy insights to address the increasing threat of post-wildfire flood effects, both in
100 terms of understanding and mitigation.

101 **2 Study area and post-wildfire flood event**

102 A Mediterranean catchment was selected as the application area: Kineta catchment in western Attica, central Greece (Fig.1).
103 It covers approximately 40 km². Its northern part is mountainous and gradually lowers to the southern part, where the coastal
104 town of Kineta is located. The climate of the Kineta catchment, like most Mediterranean areas, has hot, dry summers and mild,
105 wet winters (Kourgialas, 2021). The main land uses are forests (pine forests in the north, which were the main burned areas),
106 complex cultivation patterns with various fields in the southern part, and urban settlements (the coastal Kineta town). The
107 broader region has faced increasing wildfire risks over the past few years, with notable events in the summers of 2017 and
108 2018. These wildfires consumed the mountainous pine forest, a few houses in Kineta town and two smaller settlements, also
109 causing several injuries. Following the 2018 wildfire, protection measures primarily focused on safeguarding the road network
110 against landslides (Lekkas et al., 2019). An extreme storm event on November 24-26, 2019, led to a flash flood that caused
111 severe damage to the town of Kineta. The wildfire contributed to this flood event, as the forest and vegetation conditions had
112 not sufficiently recovered from the 2018 wildfire. Prior to the storm that caused the flood, the streams were blocked by
113 sediments accumulated since the wildfire (Lekkas et al., 2019).



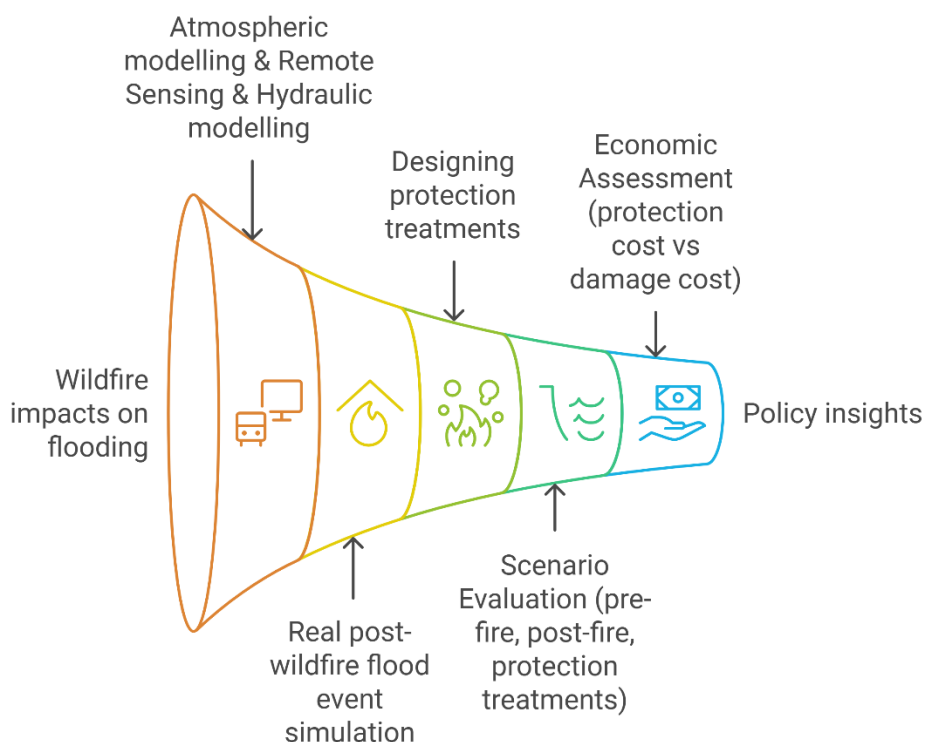


115 **Figure 1: A) The Kineta catchment's digital elevation model (DEM). Adapted from: National Cadastre and Mapping Agency S.A.**
116 **(NCMA, 2021). B) The main land cover types and the river network. C) Kineta's location in Greece (red dot). D) A picture from the**
117 **wildfire of 2018, which initiated from the mountainous part of the catchment and reached the coast. E-G) Damages caused by the**
118 **flood of 2019, affecting critical infrastructure and properties. Sources: (Lekkas et al., 2019; Protothema, 2019).**

119 **2 Materials and Methods**

120 The framework consists of the following steps (Fig.2): First, we simulate the storm that caused the studied flood event
121 (atmospheric model). Second, Remote Sensing (RS) techniques were used to identify the flooded area (flood extent) and
122 determine the burn extent and severity, which are crucial factors in assessing the wildfire's impact on the flood through altered
123 roughness coefficients. Next, we used a hydraulic model to simulate the flood event (RS-validated). We then designed the
124 PFPTs and modified the terrain in the hydraulic model to incorporate them, allowing us to run different scenarios to assess
125 their effectiveness (pre-wildfire, post-wildfire, with and without PFPTs). Finally, for each scenario, we estimated the cost of
126 the PFPTs and the direct flood damages to compare them and provide policy insights. The methodology for each step is
127 presented below.

Post-wildfire flood assessment and mitigation framework



128 **Figure 2: The general conceptual approach of the presented framework.**



130 **2.1 Atmospheric model**

131 The storm simulation was achieved by applying the Advanced Weather and Research Forecasting (WRF-ARW) v4.2 model.
132 The WRF-ARW atmospheric model has been successfully used in previous applications for simulating meteorological
133 phenomena in several case studies, including those in Greece. These applications include heavy precipitation events and
134 storms, as well as their forecasts (Alamanos et al., 2024b; Varlas et al., 2024).
135 The WRF-ARW model simulated the meteorological conditions that led to the storm of 24-25 November 2019, as presented
136 in detail in Alamanos et al. (2024b). The initialization time of the simulation was set at 00:00 UTC on November 24th (02:00
137 local time), and the simulation lasted 48 hours until 00:00 UTC on November 26th (02:00 local time). Initial and boundary
138 conditions were set using data from the Global Forecasting System (GFS) with a horizontal grid spacing of $0.25^\circ \times 0.25^\circ$. These
139 conditions involve atmospheric data across multiple layers, soil moisture, and temperature. Sea surface temperature (SST) for
140 the lower boundary conditions was updated every 6 hours, utilizing the real-time global (RTG) SST analysis dataset on a grid
141 spacing of $0.083^\circ \times 0.083^\circ$. Ground processes were parameterized through the unified Noah land surface model (Tewari et al.,
142 2004). The parameterization of the long-wave and short-wave radiation processes was based on the RRTMG scheme (Iacono
143 et al., 2008), while the cloud microphysics processes were parameterized by the WSM 5-class scheme (Hong et al., 2004).
144 Convective processes were managed by the Grell-Freitas ensemble scheme for the first domain ($9\text{km} \times 9\text{km}$) and explicit
145 convection resolution for subsequent domains ($3\text{km} \times 3\text{km}$ and $1\text{km} \times 1\text{km}$) (Grell and Freitas, 2014). Finally, the planetary
146 boundary layer and surface layer processes were resolved by the Yonsei University scheme (YSU) and the revised Monin-
147 Obukhov scheme, respectively (Hong et al., 2004).

148 **2.2 Remote sensing**

149 For the identification of the wildfire impacts and their accurate representation in the hydraulic model, we processed three
150 Sentinel-2 MSI images (one pre-fire and two post-fire) from the Copernicus Open Access Hub. Using QGIS 3.6.3 and the
151 semi-automatic classification plugin, we converted digital numbers to top-of-atmosphere reflectance and applied DOS1
152 atmospheric correction. We delineated the study area and calculated the Normalized Burn Ratio (NBR) from the NIR (B08)
153 and SWIR (B12) bands. We then derived the change in NBR (dNBR) by subtracting the post-fire values from the July 20,
154 2018, reference. Applying a +0.1 dNBR threshold and USGS-recommended burn severity classes, we produced a burn severity
155 map. By overlaying land-use data, we assigned updated Manning's n roughness coefficients to represent burned conditions in
156 the hydraulic model, as explained below. For more details, as presented also in Alamanos et al. (2024b), see Section S1 and
157 Fig. S1 in the Supporting Information (SI).

158 RS analysis was also used to obtain a picture of the actual flood extent for the November 24th event, allowing us to validate
159 the hydraulic model. We used a single Sentinel-2 image from November 25th, 2019 (Level 1C, 09:23 UTC). After converting
160 digital numbers to top-of-atmosphere reflectance and applying DOS1 atmospheric correction in QGIS, we evaluated five
161 spectral water indices (NDWI, MNDWI, AWEI, RSWIR1, and RSWIR2) and transformed SWIR2, NIR, and red bands into



162 HSV colour space. For each index, we performed histogram analysis to identify peak values (positive for water, negative or
163 zero for land) and manually adjusted thresholds to match drone footage and post-flood imagery. Binarizing each index
164 produced logical water masks, which were combined into a final inundation map. This observed flood polygon served as the
165 validation dataset for our hydraulic model (validation polygon). For more details, see Section S1 and Fig.S2 in the SI.

166 **2.3 Hydraulic - Hydrodynamic model**

167 The flash flood was modelled within the 2D Hydrologic Engineering Center's River Analysis System (HEC-RAS) (Hydrologic
168 Engineering Center (HEC), 2022). The input data was:

- 169 • The Digital Elevation Model (DEM) of the area, obtained by the National Cadastre and Mapping Agency S.A.
170 (NCMA), has a 2-m resolution to achieve fine-quality and detailed simulation even at small scales, including the
171 detailed representation of the stream network.
- 172 • The meteorological conditions were obtained from the WRF-ARW simulated precipitation. The output of WRF-ARW
173 (section 2.1) was applied as a rain-on-grid input in HEC-RAS. The rain-on-grid technique is a relatively new approach
174 that enables users to apply spatial datasets of gridded rainfall to the study area, in contrast to traditional point
175 observations (Alamanos et al., 2024b; Papaioannou et al., 2021). Therefore, 20 spatial datasets/grids were inserted
176 into HEC-RAS, representing the storm event from November 24th, 2019, at 14:00:00 to November 25th, 2019, at
177 09:00:00, using a 1-hour time step.
- 178 • The Manning's roughness coefficients (n) coefficients of the catchment. The most common approach to define n is to
179 use typical minimum, median, and maximum values from the literature for similar areas in similar conditions. We
180 considered the land cover maps (CORINE) and their overlapping burn extent areas and burnt severity classes (as
181 estimated using RS techniques – Section 2.2) (Wu et al., 2021). For each combination of land cover-burnt extent and
182 severity, we assigned n coefficients based on the literature for both the pre-wildfire and post-wildfire conditions
183 (Table S1). Following this process, the spatially distributed Manning's roughness coefficients were estimated. For
184 more details, see Section S2 and Table S1 in the SI.

185 The model provides the flood inundation (extent), water depth and velocity for each time step of the simulated event, and the
186 flood maximum arrival time in both pre-wildfire (hypothetically, if the same storm had occurred before the wildfire), and post-
187 wildfire cases, for comparison purposes. The flood extent results (validation polygon) produced by the RS techniques (Section
188 2.2) were used to validate the results of the HEC-RAS model. The accuracy of the hydraulic model was quantified using the
189 Critical Success Index (CSI), a widely recognized metric for flood inundation models (Zotou et al., 2022). The CSI takes into
190 account the correctly simulated flooded areas against the validation polygon while considering the false-simulated flooded
191 areas, as well as those areas that flooded but were not predicted by the model (Nandam and Patel, 2024). For more details, see
192 Section S3 in the SI.



193 2.4 Post-wildfire Flood Protection Treatments (PFPTs) and scenarios for evaluating their effectiveness

194 The PFPTs would aim to protect the Kineta catchment after the 2018 wildfire from upcoming extreme storm events, including
195 the 2019 flood. However, such measures were not fully in place or were only poorly installed.

196 We evaluated the most suitable PFPTs for the catchment. First, we conducted a literature review to assess all available
197 information on PFPT types and cost-effectiveness (see Section S4 and Table S2 in the SI) (Papaioannou et al., 2023). We
198 observed that the most commonly used PFPTs are land barriers and channel barriers, mainly due to technical practicality and
199 lower (installation) costs. Particularly in Greece, these refer to barrier-based log-erosion barriers (LEBs) and channel-based
200 wooden check dams (WCDs), respectively. We also reviewed the official Greek studies for PFPTs' application, which were
201 released after the 2023 wildfires in the country, suggesting such treatments for similar case studies to the Kineta catchment
202 (Greek Ministry of Environment and Energy, 2023; Koudoumakis et al., 2024). They also suggested LEBs and WCD due to
203 their low cost and ease of installation using local timber, expecting that these structures can trap sediments, reduce excess
204 flow, and slow runoff, thus protecting downstream areas from floodwaters and sediments (Alamanos et al., 2024a). Thus, we
205 designed a series of LEBs and WCD for the Kineta catchment, tailored to its size and slopes, as follows:

- 206 • 0.2-meter high LEBs (suitable for areas with moderate to high burn severity and slopes between 10%-50%) are
207 installed every 10m along the contour lines
- 208 • 1-meter high WCD (usually recommended for slight slopes <20%) are placed in the 1st, 2nd, and 3rd order streams at
209 intervals of 10m, forming a continuous line of protection also at the points of intersection with the LEBs.

210 The designed PFPTs are shown in Fig. S3 of the SI. The resulting PFPT design forms a dense and realistic network of
211 continuous 'protection lines' across streams and slopes.

212 Having designed the PFPTs spatially, we can modify the terrain of the HEC-RAS model accordingly. The terrain was modified
213 to incorporate the suggested PFPTs according to Fig.S3 using the R package "terra" to analyze the raster file with the designed
214 PFPTs (Fig.S3), the R package "sf" to analyze vectors (placing thus the LEBs and WCD in the defined intervals), and the R
215 package "smoothr" for lines smoothing, making the PFPTs suggested installation realistic (see section S4 in the SI). We then
216 run different scenarios in the HEC-RAS model:

- 217 • **Pre-wildfire, No PFPTs (wildfire effect scenario):** the same storm applies in the catchment with pre-wildfire
218 conditions, using the respective Manning's n coefficients from Table S1. No PFPTs are in place. This hypothetical
219 scenario was simulated for comparison purposes of the pre- and post-wildfire situations, aiming to isolate the effect
220 of the wildfire on flooding.
- 221 • **Post-wildfire, No PFPTs (reality scenario):** the same storm applies in the catchment with post-wildfire conditions,
222 using the respective Manning's n coefficients from Table S1. No PFPTs are in place. This is the reality of what
223 happened in Kineta, so the results of this scenario were the ones that were validated, and all roughness coefficients
224 were adjusted accordingly. In this scenario, some major culverts and bridges are blocked due to debris, similar to the
225 observed impacts of the flood.



226 • **Post-wildfire, With PFPTs (protection scenario):** the same storm applies in the catchment, with post-wildfire
227 conditions, using the respective Manning's n coefficients from Table S1, and the modified terrain that includes the
228 PFPTs, so that the designed network of LEBs and WCD is in place. This is our suggested wish-case, where protection
229 should have been considered after the wildfire, to mitigate potential future floods. In this scenario, it was assumed
230 that PFPT works would retain debris, and thus, major culverts and bridges would not be blocked.

231 The results of these scenarios were tested in terms of i) flood extent (area), ii) water depth, iii) water velocity, iv) flood
232 maximum arrival time, and v) costs and damages (analyzed in the following sections).

233

234 **2.5 Economic analysis: PFPTs cost vs Flood damage cost**

235 From an engineering perspective, post-wildfire flood resilience heavily relies on the application of necessary protection
236 measures. From an economic or policy perspective, however, the decision to apply the PFPTs is connected to the associated
237 costs (Alamanos et al., 2024a). We assess the direct economic implications of the proposed PFPTs' application by estimating
238 their total implementation cost and comparing them with the direct cost of avoided damage. Our estimations for PFPTs consider
239 the necessary material and transportation costs, as well as the installation and labour costs. This information was obtained from
240 the Greek guidelines, which provide detailed cost breakdowns for such works. For more information, see Table S2 in the SI.
241 Moreover, we present a comparison of these costs with the direct cost of avoided flood damage to provide a measure of the
242 potential value of these protection efforts. The direct damage costs caused by the flood were estimated taking into account the
243 damages that occur due to the physical contact of objects with the floodwater (Merz et al., 2004; Thielen et al., 2009), and are
244 usually straightforward to estimate (Brémond et al., 2013; Zabret et al., 2018).

245 To assess them, we counted the affected elements by the flood by inputting the flood inundation results (flooded area) into the
246 AI tool "Segment Anything Model" (SAM) (Kirillov et al., 2023), a widely used application for image segmentation. This tool
247 delineates the objects in the area (e.g. houses, commercial buildings, agricultural fields). A human check-counting was also
248 performed by navigating in Google Street Maps and comparing the results to ensure that the identified elements were complete
249 and correctly counted (see Section S5, Fig.S4, and Table S3 in the SI). Thus, this semi-automated approach involving Artificial
250 Intelligence (AI) provided us with accurate estimates of the affected properties. Then, typical insurance and monetary values
251 were used to calculate the direct flood damage costs for those affected properties (see Section S5 and Table S3 in the SI). For
252 the calculation of the economic losses due to a blocked road (Athens-Corinth highway) from flooding, we used a general
253 estimation model (Eq. S2), which takes into account factors like the daily vehicle traffic, the additional distance of detour,
254 vehicle operating costs, additional travel time, and the direct economic value of time and goods affected (see section S5, and
255 Eq.S2, in the SI). Finally, the infrastructure damages were considered (repair costs of roads, streams, land, and drainage) as
256 reported by the local authorities (see section S5, in the SI).

257 For all scenarios (Pre-wildfire, No PFPTs; post-wildfire, No PFPTs; and Post-wildfire, with PFPTs), flood damage costs were
258 estimated based on the flood extent (area-based), as we only account for direct costs. The results of the "reality" scenario (Post-
259 wildfire, No PFPTs) were validated over the official Greek estimates for restoring the damages in Kineta. For the other two

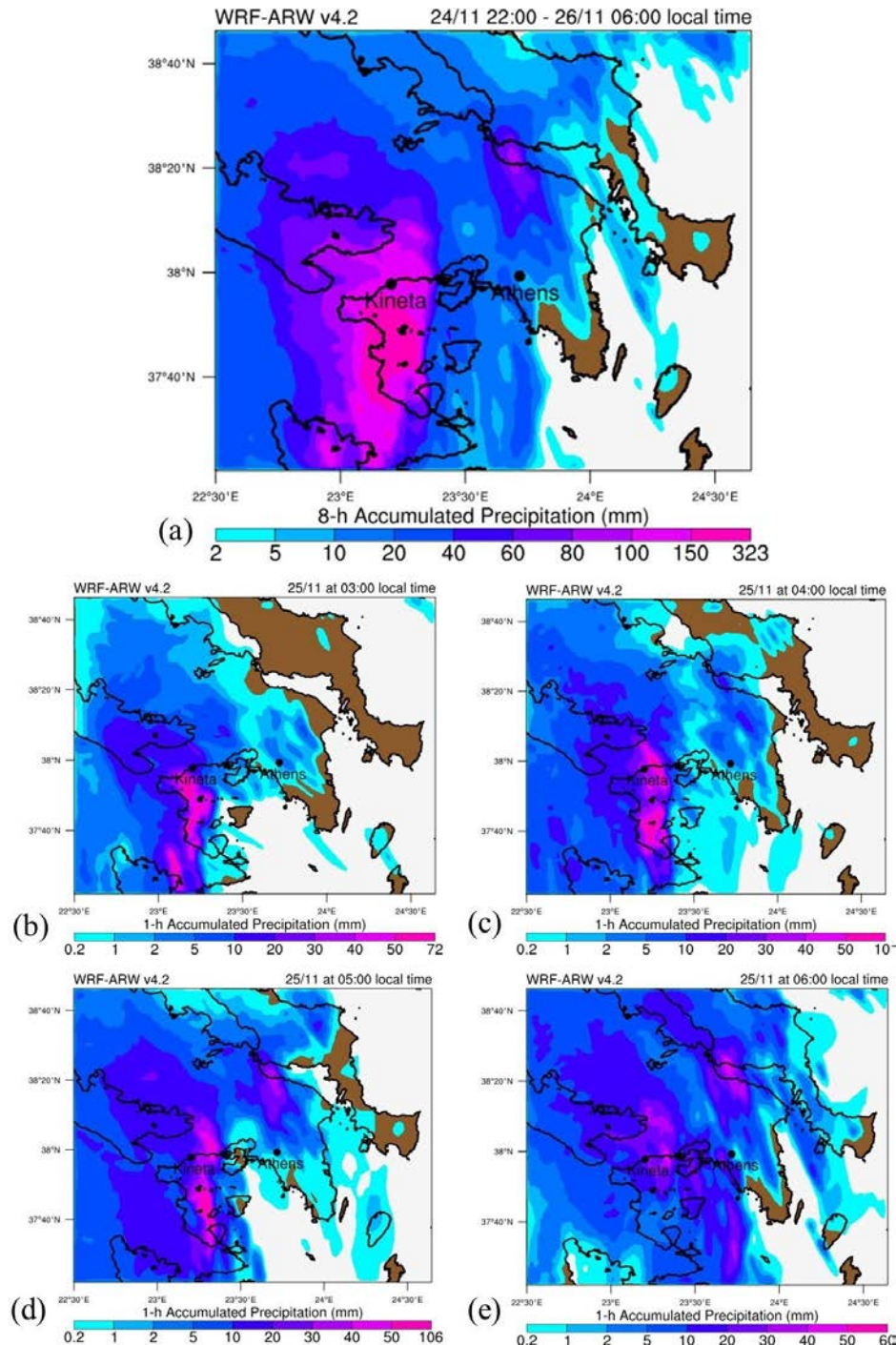


260 hypothetical scenarios (Pre-wildfire, No PFPTs and Post-wildfire, With PFPTs), we also assume that the Athens-Corinth
261 highway would have been blocked, and we follow an area-based approach to calculate the infrastructure costs.

262 **3 Results**

263 **3.1 Atmospheric model results**

264 The storm of November 24th and 25th was extreme, as a deep barometric low originating from the west led to substantial
265 precipitation across various regions in Greece. A cold front accompanying this low-pressure system triggered heavy rainfall
266 in Kineta and its neighbouring areas during the night of November 24th to 25th. The meteorological station of the National
267 Observatory of Athens (NOA) network at Agioi Theodoroi (approximately 8 kilometres southwest of Kineta) recorded a total
268 rainfall of 206.8 millimetres over the two-day period of November 24th to 25th (Meteo, 2024). The results of the WRF-ARW
269 simulation estimated a rainfall of 182.6 millimetres over the same area, aligning closely with the actual measurements. As Fig
270 3 shows, most of the precipitation occurred between November 24th, 20:00 UTC (local time 22:00), and November 25th, 06:00
271 UTC (local time 08:00). Particularly in the early morning hours of November 25th, a severe storm centred around Kineta,
272 evident from the pattern and intensity of the 1-hour accumulated precipitation (Fig.3) from 03:00 to 06:00 local time. These
273 rainfall rates led to increased runoff within the Kineta catchment, which caused the flash flood.



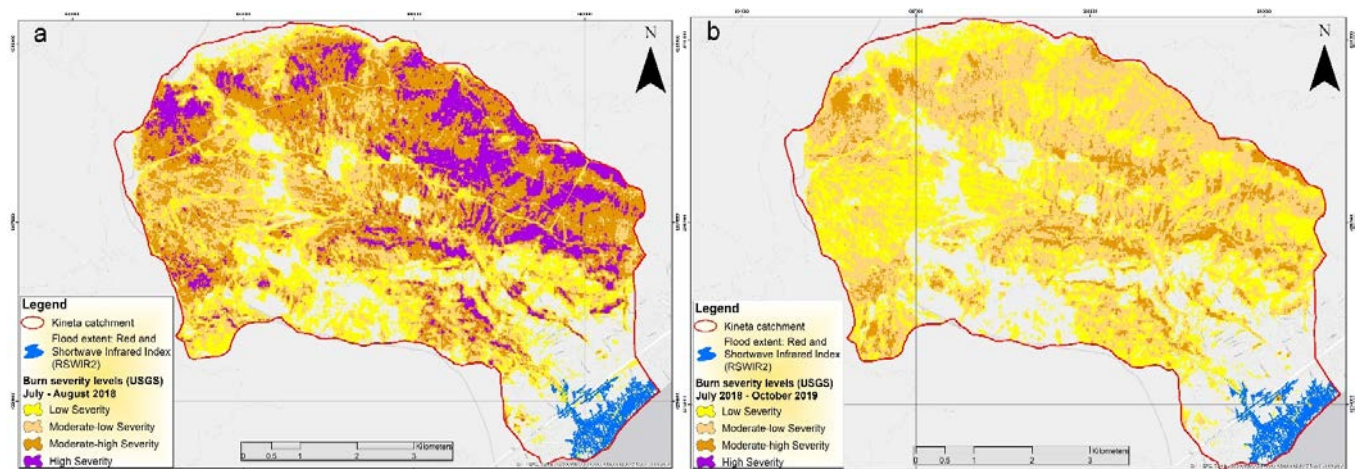
275 **Figure 3: The results of the WRF-ARW model of the simulated accumulated precipitation (in mm) for: a) 8-h for the period from**
276 **November 24th at 22:00 local time to November 25th at 06:00 local time, b) 1-h for November 25th at 03:00 local time, c) 1-h for**
277 **November 25th at 04:00 local time, d) 1-h for November 25th at 05:00 local time, and e) 1-h for November 25th at 06:00 local time.**

278 **Source: (Alamanos et al., 2024b).**



279 **3.2 Remote sensing results**

280 First, the results of the RS analysis indicated the burn severity and extent, as well as their changes during the period from the
281 wildfire until the flood event. The analysis of the dNBR revealed regrowth of vegetation after the wildfire, from August 2018
282 to October 2019, specifically just before the flood event. During this period, the proportion of unburnt areas (24.1%) and those
283 with low (29.3%) or low-moderate (35.5%) burn severity increased compared to August 2018, where the corresponding
284 percentages were 19%, 15.9%, and 21%, respectively. Furthermore, the predominant burn severity classes are those subjected
285 to moderate-high and moderate-low severity and the unburnt areas for 2018, and moderate-low and low severity and unburnt
286 area for October 2019. Notably, the extent of areas affected by high burn severity (0.01%) significantly decreased in October
287 2019 compared to August 2018 (12.5%), with these regions largely transitioning to areas impacted by moderate-low burn
288 severity (Fig.4a,b, and Fig.S1). Furthermore, the RS analysis provided us with a map of the flood extent. This was produced
289 by comparing all computed Water Indices (WIs), interpreting them with expert knowledge, and visually inspecting them while
290 aligning them with the 4 (Red)-3 (Green)-2 (Blue) natural composite of the corresponding S2 image, as described in section
291 2.2. The intensified analysis revealed that the Red and Short-Wave Infrared 2 Index (RSWIR2), with a threshold value of $\geq -$
292 0.1, outperformed other indices in detecting inundated areas (Fig.4a,b). This index consistently yielded the most stable results
293 throughout our analysis (Fig.S2).



294 **Figure 4: The RS results of the a) burn extent and severity of the wildfire period July-August 2018, b) burn extent and severity of**
295 **the post-wildfire period July 2018- October 2019, both illustrating the flood extent (November 2019) according to the RSWIR2 index.**

296

297 **3.3 Hydraulic-hydrodynamic model results**

298 The HEC-RAS model runs under the scenarios described in section 2.4 (pre-wildfire, post-wildfire, without and with PFPTs
299 in place).

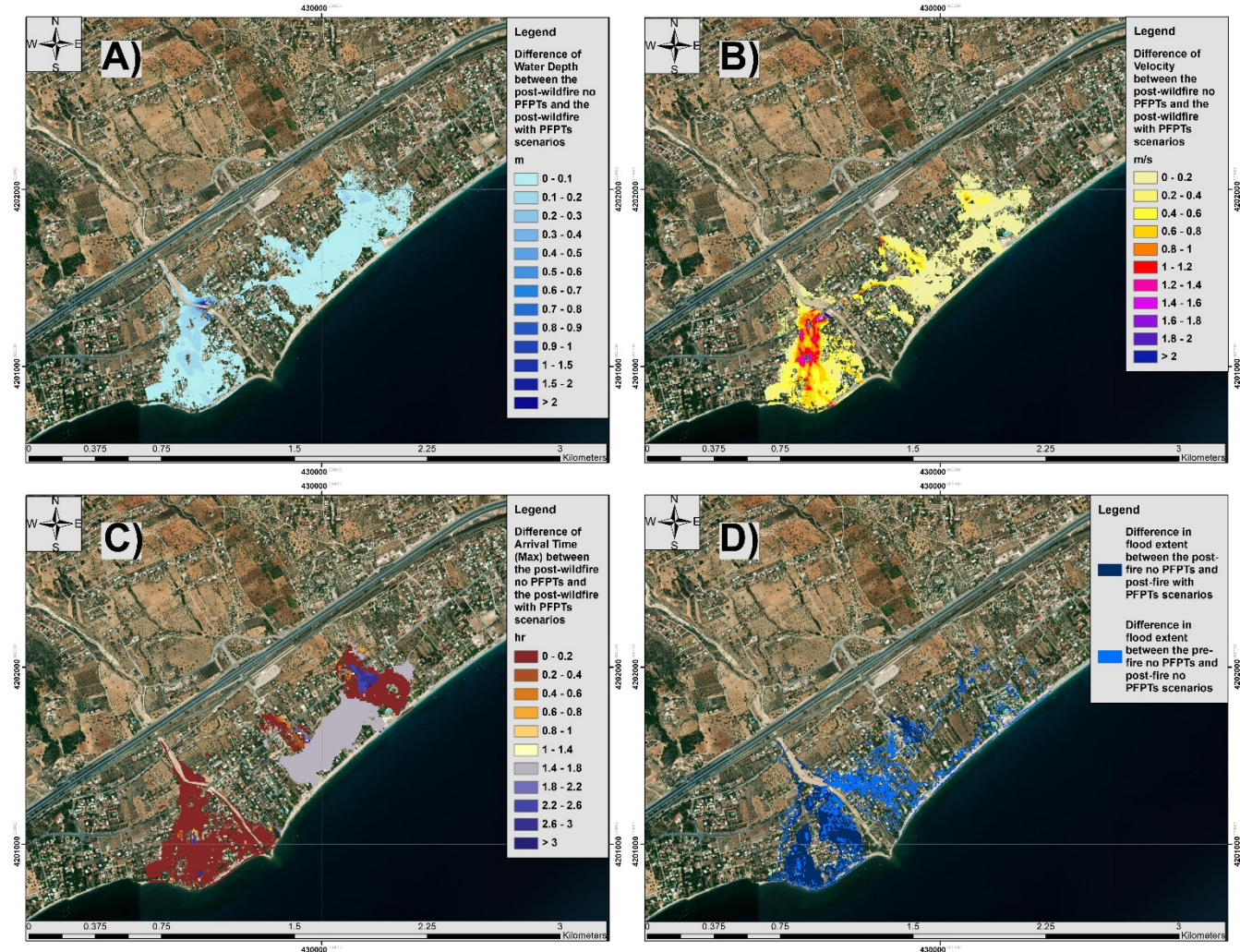


300 The model's accuracy was tested by the CSI scores, for the real case of the Post-wildfire, No PFPTs simulation, using the
301 validation polygon. The CSI score reached 0.65, indicating satisfactory performance (CSIs above 0.5 are acceptable) (Equation
302 S1) (Zotou et al., 2022).

303 The total simulated flood inundation area for the (real) post-wildfire case was 595,246 m², covering almost 24% of the town's
304 total residential area. The pre-wildfire simulation resulted in a flood inundation area of 451,848 m². The difference in these
305 flood extents reflects the impact of the wildfire on the flooding, which is 143,398 m². If the PFPTs were in place after the
306 wildfire, the flood extent would have been 447,575 m². Therefore, the effect of these recommended protection measures would
307 have reduced the flood-inundated area by 147,671 m² (24.8%) (see detailed results in Fig. S5). It is worth noting that this
308 difference indicates that the effect of the wildfire could have been entirely avoided with the PFPTs.

309 Figure 5 shows the differences between the reality and the protection scenarios (isolating the effect of the PFPTs), as detailed
310 in Fig.S5 and Fig.S6. We observe that the PFPTs lead to moderate reductions in peak water depths across much of the inundated
311 zone, of around 0.1-0.3m, with the biggest differences being in the peripheral areas, and in the central stream (Fig5A). Velocity
312 reductions are spatially heterogeneous but pronounced where flow paths concentrate (Fig5B). Yellow to orange zones (0.2-
313 0.8 m/s reductions) follow main overland flow corridors, while even bigger reductions (1.0-1.6 m/s, red-pink) are observed in
314 the main stream's flooding, and the rest of the broad flat areas exhibit minor reductions (0-0.2 m/s, pale yellow). Such
315 reductions, especially to the west part, can significantly reduce infrastructure damages.

316



317

318 **Figure 5: Assessment of the effect of the PFPTs on: A) Water depth, B) water velocity, C) Flood maximum arrival time, D) water**
319 **extents. These are presented as the differences between the Post-wildfire No PFTs and Post-wildfire With PFPTs, while for the**
320 **floodwater extent (D) we compare all scenarios. Base-map source: © Google Earth.**

321

322 The PFPTs introduce meaningful delays in flood wave arrival, as seen in the arrival-time difference map (Fig5C). Peripheral
323 urban areas and floodplain margins experience minimal delays (0-0.4 h, brown–light orange), while central zones downstream
324 of barrier clusters show delays of 1.0-2.2 h (light purple to deep blue). The central part of the city, which appears to be the
325 most flood-prone, had the largest delays due to PFPTs, and this is crucial for emergency response, evacuation, traffic
326 management, and individual protection measures. Moreover, elongated travel times reduce flood peaks, lessen hydraulic loads
327 on downstream structures, and allow more water to infiltrate or be retained, showcasing PFPTs' role in temporal flood risk
328 mitigation.



329 Regarding the flood extent, the dark blue areas would have been inundated without PFPTs but remain dry when they're in
330 place. The blue shading shows the additional flood extent caused by the wildfire (post-wildfire with PFPTs vs. pre-wildfire
331 without PFPTs), underscoring how burn-induced changes expand inundation inland. This joint comparison illustrates that
332 while the post-wildfire landscape is inherently more flood-prone, strategically placed PFPTs can reclaim substantial areas from
333 inundation.

334 **3.4 Cost of protection and flood damage direct costs**

335 The estimation of the cost of the recommended PFPTs considers the typical expenses for materials (wood), transportation, and
336 construction (installation), in values of €2023, according to the official Greek techno-economic specifications (Table S3).
337 Based on these estimations, the costs for the PFPTs designed for the Kineta catchment would be 4.87€ per meter of LEBs
338 installed, and 49.25 €m² of wooden check dams. The spatial model for the proposed PFPTs (Fig.S3) resulted in 636,049 m of
339 LEBs and 2065 wooden check dams (of an average installed area of 3.5 m²). Therefore, their total cost would be:

- 340 • 4.87€/m · 636,049 m of LEBs installed = €3.1mill, plus
- 341 • 49.25 €m² · 2065 wooden check dams · 3.5 m² each = 355,954€

342 Which, in total, sums to €3.45mill.

343 The total estimated flood damage cost considered residential house properties, commercial buildings (namely hotels in the
344 area), private vehicles, agricultural fields, the closure of the Athens-Corinth highway for an entire working day, and reported
345 infrastructure damages to roads, streams, land, and drainage. A semi-automated AI image segmentation and human counting
346 approach was applied to count the affected elements, and we assigned monetary values to them based on insurance data. For
347 the highway closure due to the flood, a general estimation model for such economic losses was applied (see Eq.S2 in the SI).
348 This applied to all scenarios, given the severity of the flood, with the water reaching up to the road in all simulations. The
349 infrastructure cost was adjusted based on the flooded area of each scenario.

350 The resulting total cost of €25.2mill was cross-checked and validated over the estimates of the West Attica's Region Technical
351 Works Observatory on the total repair costs (which was reported to be €21.6mill) (West Attica Region, 2021). The total
352 estimated cost, considering all these components is €25.2mill.

353 The results of the PFPTs costs and flood damages are summarized as follows:

- 354 • **Pre-wildfire, No PFPTs:** Reduced count of residential homes, commercial buildings (hotels), private vehicles, and
355 agricultural fields affected compared to the "reality" scenario; Same cost for the same highway closure; Reduced
356 infrastructure cost based on the reduced flooded area, compared to the "reality" scenario. Cost of PFPTs = 0€ Flood
357 damage cost = €19.1mill. The difference in the flood damage cost is 6,136,996€ (or 24.33% of the real event's
358 damage), which is purely attributed to the wildfire.
- 359 • **Post-wildfire, No PFPTs:** The exact affected number of residential homes, commercial buildings (hotels), private
360 vehicles, and agricultural fields; Actual cost for the Athens-Corinth highway closure; Actual infrastructure cost. Cost
361 of PFPTs = 0€ Flood damage cost = €25.2mill. This represents the real case, which highlights the extensive financial



362 burden on local authorities and communities, underscoring the need for effective flood management and mitigation
363 strategies to reduce long-term economic impacts.

364 • **Post-wildfire, With PFPTs:** Reduced count of residential homes, commercial buildings (hotels), private vehicles,
365 and agricultural fields; Same cost for the same highway closure; Reduced infrastructure cost based on the reduced
366 flooded area. Cost of PFPTs = €3.45mill, Flood damage cost = €18.9mill. The difference in the flood damage cost is
367 €6.4mill. This indicates that the PFPTs could have reduced the actual real case's flood damage costs by 25.3%,
368 completely offsetting the wildfire's impact.

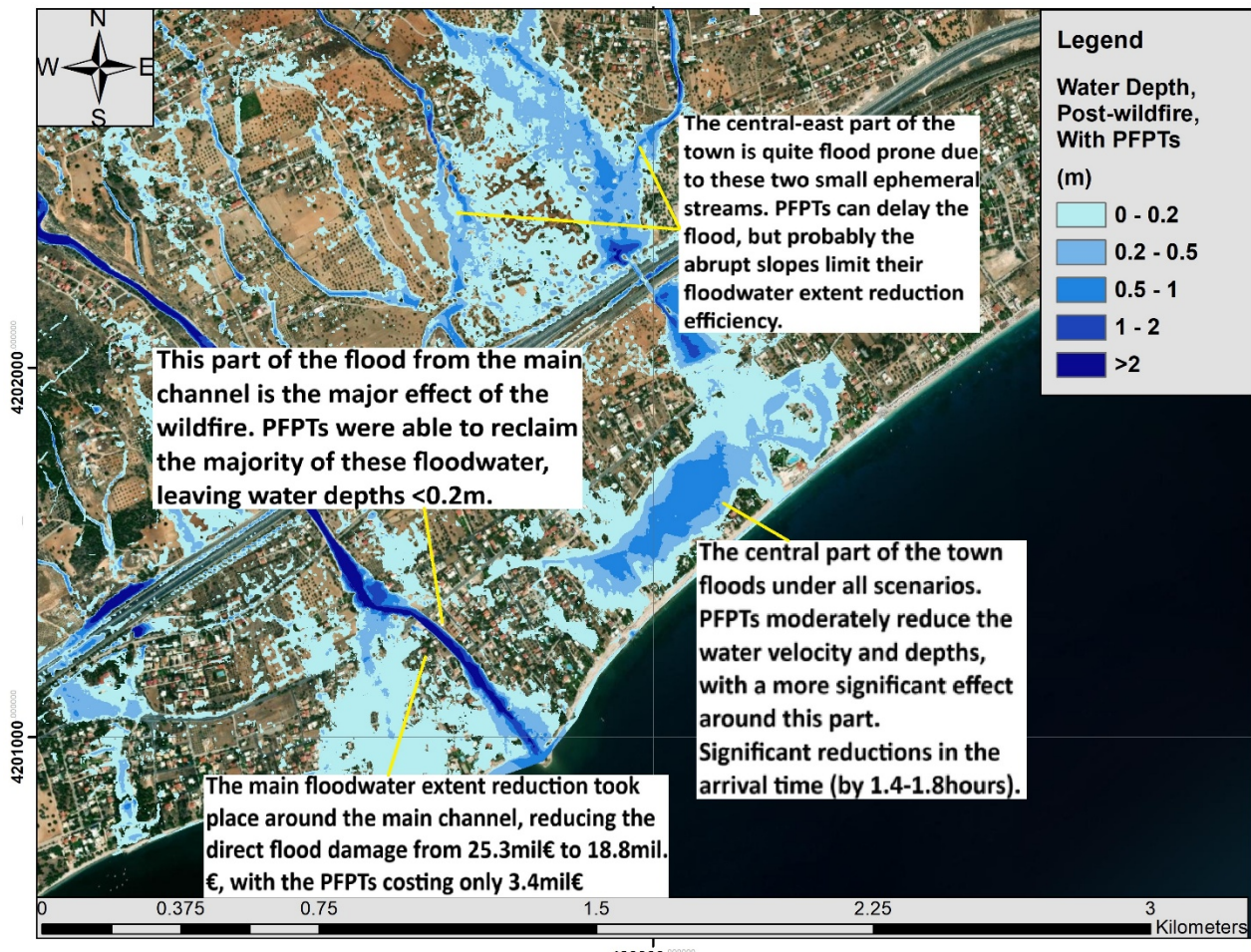
369 **4 Discussion**

370 **4.1 Modelling post-wildfire floods and PFPTs**

371 The representation of the post-wildfire flood event, considering a combination of methods (meteorologic model, RS, hydraulic-
372 hydrodynamic, and spatial PFPTs-design model) is a challenging and interdisciplinary modelling task. With this combined
373 modelling approach, on the one hand, we provide a framework for similar analyses, as all models are freely available and can
374 be used in combination (soft-linked) to represent other post-wildfire flood events. On the other hand, this approach led to
375 accurate representation that enables building on the findings (flood inundation maps) to consider protection measures and
376 enhance resilience. Also, the modelling of the PFPTs within HEC-RAS is a novel application. An interesting set of findings
377 here is the wildfire's and the PFPTs' effects on flooding. The effect of the wildfire on the flood extent is 24.1% (difference of
378 the pre- and post-wildfire scenarios), which is not negligible for a small town. Regarding the effectiveness of the PFPTs, if the
379 recommended measures were in place, 24.8% of the flooding would have been avoided, while most of the floodwaters would
380 have been delayed, coming with reduced velocities and depths.

381 **4.2 Exploring the effect of PFPTs**

382 The analysis for the application of the most suitable PFPTs, their mapping, and cost-effectiveness is also a challenging task,
383 as the literature on PFPTs is limited. To the best of our knowledge, this is the first attempt to model PFPTs based on spatially
384 modelled physical characteristics and case-study-specific technical guidelines, along with a detailed assessment of their cost-
385 effectiveness for flood mitigation. This approach illustrates how the PFPTs can be followed to other study areas, similarly, and
386 give at least a preliminary picture/estimation of the potential post-wildfire measures. As mentioned, their effectiveness is
387 significant, completely offsetting the wildfire's impact on flooding. Especially if we consider the significance of the
388 downstream residential area, and take into account the overall effects in water extent, depth, velocity, and arrival times, as well
389 as the relatively low costs, there is no doubt on the PFPTs' value.



392
393 **Figure 6: Summarizing the main findings on the effect of PFPTs, over the Post-wildfire With PFPTs scenario. Base-map source: ©**
394 **Google Earth.**

395

396 Overall, as Fig.6 summarizes, the PFPTs are particularly effective along the main stream, where well-established flowpaths
397 and gentle slopes allow LEBs and WCD to intercept and attenuate floodwaters over long reaches. This configuration not only
398 reduces peak velocities but also meaningfully delays water arrival times, offering valuable lead-time for downstream
399 communities. In contrast, PFPTs prove less efficient in the smaller Intermittent Rivers and Ephemeral Streams (IRES) in the
400 northeast part of the catchment with steeper, more abrupt slopes. These were responsible for the majority of the flooding,
401 indicating the need to map IRES, as they are not mapped in Greece (Pastor et al., 2022), and usually not considered in flood
402 protection plans, however, as proved, these can cause severe damages, under all scenarios. Yet even here PFPTs can
403 substantially slow the initial flood buildup, providing critical flood delay in the town centre.

404 It is worth noting that the storm of November 2019 was a severe phenomenon, that would have caused flooding under all
405 scenarios, underscoring the vulnerability of the area, and the need of perhaps even more strict flood protection works. The



406 PFPTs largely mitigate the wildfire's hydrological impact, rather than the flood event itself: even under pre-wildfire conditions,
407 this storm was severe enough to inundate much of the floodplain. Thus, additional and more robust flood defences remain
408 essential for events of this magnitude.

409

410 **4.3 Economic assessment**

411 The cost of the PFPTs, the flood damage direct cost, and ultimately their comparison, were insightful for the cost-effectiveness
412 of protection investments. The cost of the examined PFPTs resulted to €3.45mill, while the direct flood damage cost was
413 estimated to €25.2mill (around 7.5 times higher). This indicates a considerable difference, with the cost of the measures aiming
414 to the flood damage mitigation (PFPTs) being just the 13.7% of (only) the direct flood damage costs. This is a 'lesson in
415 preparedness', highlighting that investing in mitigation works can help reducing much larger hazard-induced damages.

416 At this point, the limitations should be mentioned. Due to unavailable data, we did not consider certain components of the
417 flood damage cost – in particular, those beyond the direct costs: The economic impact of business interruption caused by the
418 flood (this includes lost revenue, additional expenses incurred due to downtime, and potential long-term impacts on business
419 operations) has not been considered. Moreover, the health impacts of the flood, including medical expenses, emergency
420 response costs, and potential long-term health effects were not taken into account in the flood damage cost estimations. Other
421 environmental damages such as pollution, habitat destruction, and cleanup costs, were not considered. Finally, the community
422 and social costs were also ignored (including displacement of residents, loss of community services, and psychological effects).
423 So, our flood damage cost estimates are quite conservative (just the direct costs), and in reality, they are way higher –
424 significantly more than five times the investment in post-wildfire flood protection. Moreover, the flood damage estimation
425 was primarily based on the flooded area. In the protection scenario (Post-wildfire, With PFPTs), we observed that even if there
426 was floodwater in some parts, the depth was lower than 20-10cm, and the velocity was also negligible, indicating that in reality
427 the damage cost might have been less than €18.9mill. At the same time, the PFPT measures proposed for the case of Kineta
428 are also conservative (i.e., a dense network of LEBs and wooden check-dams was proposed), but other approaches might
429 consider less PFPTs, significantly lowering their costs. Having a 'low-end' estimate of flood damage cost, and a 'high-end'
430 estimate of the PFPTs' costs, and still proving their significant difference, highlights even more the fact that 'precaution' seems
431 to be a wiser decision than 'cure'.

432 **5 Conclusions**

433 The findings of this modelling study, beyond the general framework provided for the integrated analysis of similar phenomena,
434 show the importance of investing in the flood resilience of burnt sites. This study showed that the PFPTs would have been able
435 to reduce a substantial floodwater amount, somewhat larger than the entire flood that was due to the wildfire. Of course, this
436 does not mean that if the PFPTs had been in place after the wildfire, the flood would have been totally avoided. In other words,
437 the investment of approximately €3.45mill would not have been enough to avoid the €25.2mill flood damage cost. However,



438 the flood would have been mitigated, saving at least €7 mill from the damages. Again, this estimate is quite conservative, as
439 explained in the discussion section; therefore, we believe that the investment in preparedness is definitely worthwhile. For
440 now, our findings can provide food for thought and serve as a lesson in preparedness, indicating that post-wildfire flood
441 protection can be a cost-effective decision, relatively inexpensive, and can be achieved at local scales (e.g., at the municipality
442 scale) with local means.

443 A follow-up question from this research is on the need to map the IRES, and those like the one in Kineta that have abrupt
444 slopes, to consider enhanced protection measures. Another follow-up question is, although the studied storm was indeed
445 extreme and caused a flood under all scenarios, why are these protection measures not applied to mitigate it? One possible
446 explanation is limited awareness among decision-makers, combined with weak communication and possibly lack of trust
447 between authorities and experts who hold relevant knowledge. Another explanation could be that decision-makers consider
448 PFPTs as an expensive objective compared to flood damage costs, which will not likely grab headlines (in contrast to news
449 reporting a big fire or flood) (Nature Sustainability, 2023). Following the wildfires in Kineta, Greek newspapers argued that a
450 significant investment in preventive measures is necessary to address future flood risks, noting that even after the flood, there
451 was still no protection work in place (Chaini, 2019). Often, flood damage compensation is not being paid in Greece, and
452 restoration works are being significantly delayed. This also occurred in Kineta, where the latest reports on the case indicate
453 that the compensation for the affected households was still pending (Papadopoulou, 2025). Therefore, if there is a tendency to
454 dismiss flood damage compensation, then the application of PFPTs seems indeed like an unnecessary and undesirable expense.
455 At the end of 2024, after extended protests, the case of Kineta was brought to court, as no PFPTs were in place, nor
456 compensations were granted. The primary defendant is the Former Regional Governor of Attica, and the case is underway
457 (Prothema, 2024).

458 Further science-to-policy bridges and collaboration can significantly improve our understanding of complex hazards, such as
459 post-wildfire floods, an often-overlooked topic, and assess the potential of PFPTs, while highlighting the need for timely
460 resilience-building and preparedness as a necessary step, rather than inaction.

461 **References**

462 Alamanos, A.: Exploring the Impact of Future Land Uses on Flood Risks and Ecosystem Services, With Limited Data:
463 Coupling a Cellular Automata Markov (CAM) Model, With Hydraulic and Spatial Valuation Models, *Qeios*,
464 <https://doi.org/10.32388/JJWWBD>, 2024.

465 Alamanos, A., Papaioannou, G., Varlas, G., Markogianni, V., Plataniotis, A., Papadopoulos, A., Dimitriou, E., and Koundouri,
466 P.: Designing Post-Fire Flood Protection Techniques for a Real Event in Central Greece, *Prevention and Treatment of Natural*
467 *Disasters*, 3, 2024a.

468 Alamanos, A., Papaioannou, G., Varlas, G., Markogianni, V., Papadopoulos, A., and Dimitriou, E.: Representation of a Post-
469 Fire Flash-Flood Event Combining Meteorological Simulations, Remote Sensing, and Hydraulic Modeling, *Land*, 13, 47,
470 <https://doi.org/10.3390/land13010047>, 2024b.



471 Nature Sustainability: Time to recover, *Nat Sustain*, 6, 1027–1027, <https://doi.org/10.1038/s41893-023-01228-z>, 2023.

472 Basheer, M. and Oommen, T.: PyLandslide: A Python tool for landslide susceptibility mapping and uncertainty analysis, *Environmental Modelling & Software*, 177, 106055, <https://doi.org/10.1016/j.envsoft.2024.106055>, 2024.

474 Brémond, P., Grelot, F., and Agenais, A.-L.: Review Article: Economic evaluation of flood damage to agriculture – review
475 and analysis of existing methods, *Natural Hazards and Earth System Sciences*, 13, 2493–2512, <https://doi.org/10.5194/nhess-13-2493-2013>, 2013.

477 Brogan, D. J., MacDonald, L. H., Nelson, P. A., and Morgan, J. A.: Geomorphic complexity and sensitivity in channels to fire
478 and floods in mountain catchments, *Geomorphology*, 337, 53–68, <https://doi.org/10.1016/j.geomorph.2019.03.031>, 2019a.

479 Brogan, D. J., Nelson, P. A., and MacDonald, L. H.: Spatial and temporal patterns of sediment storage and erosion following
480 a wildfire and extreme flood, *Earth Surface Dynamics*, 7, 563–590, <https://doi.org/10.5194/esurf-7-563-2019>, 2019b.

481 Chaini, A.: No flood protection works in Kineta: the causes of the disaster, *Ecozen*, 2019.

482 Chrysovergis, P., Chrysovergis, S., and Chrysovergis, T.: An Evaluation of Post-Wildfire Erosional and Flooding Damage in
483 Southern California, 116–128, <https://doi.org/10.1061/9780784483688.012>, 2021.

484 Cos, J., Doblas-Reyes, F., Jury, M., Marcos, R., Bretonnière, P.-A., and Samsó, M.: The Mediterranean climate change hotspot
485 in the CMIP5 and CMIP6 projections, *Earth System Dynamics*, 13, 321–340, <https://doi.org/10.5194/esd-13-321-2022>, 2022.

486 Ebel, B. A. and Martin, D. A.: Meta-analysis of field-saturated hydraulic conductivity recovery following wildland fire:
487 Applications for hydrologic model parameterization and resilience assessment, *Hydrological Processes*, 31, 3682–3696,
488 <https://doi.org/10.1002/hyp.11288>, 2017.

489 Girona-García, A., Vieira, D. C. S., Silva, J., Fernández, C., Robichaud, P. R., and Keizer, J. J.: Effectiveness of post-fire soil
490 erosion mitigation treatments: A systematic review and meta-analysis, *Earth-Science Reviews*, 217, 103611,
491 <https://doi.org/10.1016/j.earscirev.2021.103611>, 2021.

492 Girona-García, A., Cretella, C., Fernández, C., Robichaud, P. R., Vieira, D. C. S., and Keizer, J. J.: How much does it cost to
493 mitigate soil erosion after wildfires?, *J Environ Manage*, 334, 117478, <https://doi.org/10.1016/j.jenvman.2023.117478>, 2023.

494 Godara, N., Bruland, O., and Alfredsen, K.: Simulation of flash flood peaks in a small and steep catchment using rain-on-grid
495 technique, *Journal of Flood Risk Management*, 16, e12898, <https://doi.org/10.1111/jfr3.12898>, 2023.

496 Greek Ministry of Environment and Energy: Study on soil-erosion and flood protection works at the burnt area of the Avantas
497 catchment and surrounding settlements. Decentralized Administration of Macedonia and Thrace. (in Greek), 2023.

498 Grell, G. A. and Freitas, S. R.: A scale and aerosol aware stochastic convective parameterization for weather and air quality
499 modeling, *Atmospheric Chemistry and Physics*, 14, 5233–5250, <https://doi.org/10.5194/acp-14-5233-2014>, 2014.

500 Hasan, M. M., Burian, S., and Barber, M. E.: Determining The Impacts Of Wildfires On Peak Flood Flows In High Mountain
501 Watersheds, *International Journal of Environmental Impacts*, 3(2020), 12, <https://doi.org/10.2495/EI-V3-N4-339-351>, 2020.

502 Havel, A., Tasdighi, A., and Arabi, M.: Assessing the hydrologic response to wildfires in mountainous regions, *Hydrology*
503 and Earth System Sciences, 22, 2527–2550, <https://doi.org/10.5194/hess-22-2527-2018>, 2018.



504 Hong, S.-Y., Dudhia, J., and Chen, S.-H.: A Revised Approach to Ice Microphysical Processes for the Bulk Parameterization
505 of Clouds and Precipitation, *Monthly Weather Review*, 132, 103–120, [https://doi.org/10.1175/1520-0493\(2004\)132<0103:ARATIM>2.0.CO;2](https://doi.org/10.1175/1520-0493(2004)132<0103:ARATIM>2.0.CO;2), 2004.

507 Hydrologic Engineering Center (HEC): River Analysis Systems - HEC-RAS (Version 6.3.1). U.S. Army Corps of Engineers.,
508 2022.

509 Iacono, M. J., Delamere, J. S., Mlawer, E. J., Shephard, M. W., Clough, S. A., and Collins, W. D.: Radiative forcing by long-
510 lived greenhouse gases: Calculations with the AER radiative transfer models, *Journal of Geophysical Research: Atmospheres*,
511 113, <https://doi.org/10.1029/2008JD009944>, 2008.

512 Kastridis, A. and Kamperidou, V.: Evaluation of the post-fire erosion and flood control works in the area of Cassandra
513 (Chalkidiki, North Greece), *J. For. Res.*, 26, 209–217, <https://doi.org/10.1007/s11676-014-0005-9>, 2015.

514 Kirillov, A., Mintun, E., Ravi, N., Mao, H., Rolland, C., Gustafson, L., Xiao, T., Whitehead, S., Berg, A. C., Lo, W.-Y., Dollár,
515 P., and Girshick, R.: Segment Anything, <https://doi.org/10.48550/arXiv.2304.02643>, April 5th 2023.

516 Koudoumakis, P., Keramitsoglou, K., Protopapas, A. L., and Dokas, I.: A general method for multi-hazard intensity
517 assessment for cultural resources: Implementation in the region of Eastern Macedonia and Thrace, Greece, *International
518 Journal of Disaster Risk Reduction*, 100, 104197, <https://doi.org/10.1016/j.ijdrr.2023.104197>, 2024.

519 Kourgialas, N. N.: A critical review of water resources in Greece: The key role of agricultural adaptation to climate-water
520 effects, *Science of The Total Environment*, 775, 145857, <https://doi.org/10.1016/j.scitotenv.2021.145857>, 2021.

521 Lekkas, E., Spyrou, N., Filis, C., Diakakis, M., Vassilakis, E., Katsetsiadou, A., Milius, D., Arianoutsou, M., Faragitakis, G.,
522 Christopoulou, A., and Antoniou, V.: The November 25th, 2019 Kineta (Western Attica) Flood., Athens, Greece, 2019.

523 Merz, B., Kreibich, H., Thielen, A., and Schmidtke, R.: Estimation uncertainty of direct monetary flood damage to buildings,
524 *Natural Hazards and Earth System Sciences*, 4, 153–163, <https://doi.org/10.5194/nhess-4-153-2004>, 2004.

525 Meteosearch | Weather Data Portal: <https://meteosearch.meteo.gr/>, last access: April 13th 2024.

526 Mitsopoulos, G., Diakakis, M., Panagiotatou, E., Sant, V., Bloutsos, A., Lekkas, E., Baltas, E., and Stamou, A. I.: 'How would
527 an extreme flood have behaved if flood protection works were built?' the case of the disastrous flash flood of November 2017
528 in Mandra, Attica, Greece, *Urban Water Journal*, 19, 911–921, <https://doi.org/10.1080/1573062X.2022.2103002>, 2022.

529 Nandam, V. and Patel, P. L.: A framework to assess suitability of global digital elevation models for hydrodynamic modelling
530 in data scarce regions, *Journal of Hydrology*, 630, 130654, <https://doi.org/10.1016/j.jhydrol.2024.130654>, 2024.

531 Napper, C.: Burned Area Emergency Response Treatments (BAER) Catalog; US Forest Service: Washington, DC, USA; San
532 Dimas Technology and Development Center: San Dimas, CA, USA., 2006.

533 NCMA (2021). National Cadastre and Mapping Agency S.A. (NCMA).

534 Papadopoulou, A. (2025). Shocking testimonies about the flood in Kineta in 2019:
535 https://www.efsyn.gr/ellada/dikaiosyni/456701_sygklonistikes-martyries-gia-tin-plimmyra-stin-kineta-2019#goog_rewarded, last access: March 25th 2025.



537 Papaioannou, G., Vasiliades, L., Loukas, A., Alamanos, A., Efstratiadis, A., Koukouvinos, A., Tsoukalas, I., and Kossieris, P.:
538 A Flood Inundation Modeling Approach for Urban and Rural Areas in Lake and Large-Scale River Basins, *Water*, 13, 1264,
539 https://doi.org/10.3390/w13091264, 2021.

540 Papaioannou, G., Alamanos, A., and Maris, F.: Evaluating Post-Fire Erosion and Flood Protection Techniques: A Narrative
541 Review of Applications, *GeoHazards*, 4, 380–405, https://doi.org/10.3390/geohazards4040022, 2023.

542 Pastor, A. V., Tzoraki, O., Bruno, D., Kaletová, T., Mendoza-Lera, C., Alamanos, A., Brummer, M., Datry, T., De Girolamo,
543 A. M., Jakubínský, J., Logar, I., Loures, L., Ilhéu, M., Koundouri, P., Nunes, J. P., Quintas-Soriano, C., Sykes, T., Truchy, A.,
544 Tsani, S., and Jordà-Capdevila, D.: Rethinking ecosystem service indicators for their application to intermittent rivers,
545 *Ecological Indicators*, 137, 108693, https://doi.org/10.1016/j.ecolind.2022.108693, 2022.

546 Posner, A. J. and Georgakakos, K. P.: Quantifying the impact of community-scale flood mitigation, *International Journal of
547 Disaster Risk Reduction*, 24, 189–208, https://doi.org/10.1016/j.ijdrr.2017.06.001, 2017.

548 Protothema: Storm "Girionis": How Kineta was burned - Visual inspection in the area, ProtoThema, 25th November, 2019.

549 Protothema: The trial for the Kineta flood begins this autumn. Patoulis to be the first defendant., Athens, Greece, 2024.

550 Robinne, F.-N., Hallema, D. W., Bladon, K. D., and Buttle, J. M.: Wildfire impacts on hydrologic ecosystem services in North
551 American high-latitude forests: A scoping review, *Journal of Hydrology*, 581, 124360,
552 https://doi.org/10.1016/j.jhydrol.2019.124360, 2020.

553 Tewari, M., Boulder, C., Chen, F., Wang, W., Dudhia, J., LeMone, M., Mitchell, K., Ek, M., Gayno, G., Wegiel, J., and
554 Cuenca, R.: Implementation and verification of the unified Noah land surface model in the WRF model, in: 20th Conference
555 on Weather Analysis and Forecasting/16th Conference on Numerical Weather Prediction, 20th Conference on Weather
556 Analysis and Forecasting/16th Conference on Numerical Weather Prediction, 2004.

557 Theochari, A.-P. and Baltas, E.: Holistic hydrological approach to the fire event on August 2021 in Evia, Greece, *Euro-Mediterr
558 J Environ Integr*, 7, 287–298, https://doi.org/10.1007/s41207-022-00304-8, 2022.

559 Thielen, A. H., Ackermann, V., Elmer, F., Kreibich, H., Kuhlmann, B., Kunert, U., Maiwald, H., Merz, B., Müller, M., Piroth,
560 K., Schwarz, J., Schwarze, R., Seifert, I., and Seifert, J.: Methods for the evaluation of direct and indirect flood losses, *RIMAX
561 Contributions at the 4th International Symposium on Flood Defence (ISFD4)*, 2009.

562 Varlas, G., Papadopoulos, A., Papaioannou, G., Markogianni, V., Alamanos, A., and Dimitriou, E.: Integrating Ensemble
563 Weather Predictions in a Hydrologic-Hydraulic Modelling System for Fine-Resolution Flood Forecasting: The Case of Skala
564 Bridge at Evrotas River, Greece, *Atmosphere*, 15, 120, https://doi.org/10.3390/atmos15010120, 2024.

565 Wang, J., Stern, M. A., King, V. M., Alpers, C. N., Quinn, N. W. T., Flint, A. L., and Flint, L. E.: PFHydro: A New Watershed-
566 Scale Model for Post-Fire Runoff Simulation, *Environmental Modelling & Software*, 123, 104555,
567 https://doi.org/10.1016/j.envsoft.2019.104555, 2020.

568 West Attica Region: Restoration of damages for the local community of Kineta. West Attica's Technical Works Observatory.,
569 2021.

570 Wu, J., Nunes, J. P., Baartman, J. E. M., and Faúndez Urbina, C. A.: Testing the impacts of wildfire on hydrological and
571 sediment response using the OpenLISEM model. Part 1: Calibration and evaluation for a burned Mediterranean forest
572 catchment, *CATENA*, 207, 105658, https://doi.org/10.1016/j.catena.2021.105658, 2021.



573 Zabret, K., Hozjan, U., Kryžanowsky, A., Brilly, M., and Vidmar, A.: Development of model for the estimation of direct flood
574 damage including the movable property, Journal of Flood Risk Management, 11, S527–S540,
575 <https://doi.org/10.1111/jfr3.12255>, 2018.

576 Zotou, I., Karamvasis, K., Karathanassi, V., and Tsirhrintzis, V. A.: Potential of Two SAR-Based Flood Mapping Approaches
577 in Supporting an Integrated 1D/2D HEC-RAS Model, Water, 14, 4020, <https://doi.org/10.3390/w14244020>, 2022.